Computational Geosciences (2005) 9:29–59
DOI 10.1007/s10596-005-5663-4

A front-tracking method for the simulation of three-phase flow in porous media

K.-A. Lie [a] and R. Juanes [b]

[a] *SINTEF ICT, Department of Applied Mathematics, P.O. Box 124 Blindern, NO-0314 Oslo, Norway*
E-mail: Knut-Andreas.Lie@sintef.no
[b] *Stanford University, Department of Petroleum Engineering, 65 Green Earth Sciences Bldg., Stanford, CA 94305, USA*
E-mail: ruben.juanes@stanford.edu

Received 4 July 2004; accepted 31 March 2005

Under certain physically reasonable assumptions, three-phase flow of immiscible, incompressible fluids can be described by a 2×2 nongenuinely nonlinear, hyperbolic system. We combine analytical solutions to the corresponding Riemann problem with an efficient front-tracking method to study Cauchy and initial-boundary value problems. Unlike finite difference methods, the front-tracking method treats all waves as discontinuities by evolving shocks exactly and approximating rarefactions by small entropy-violating discontinuities. This way, the method can track individual waves and give very accurate (or even exact) resolution of discontinuities. We demonstrate the applicability of the method through several numerical examples, including a streamline simulation of a water-alternating-gas (WAG) injection process in a three-dimensional, heterogeneous, shallow-marine formation.

Keywords: detached-branches, front-tracking, porous media, Riemann problem, shock, streamline simulation, three-phase flow, water-alternating-gas

1. Introduction

It is by now well established that most oil recovery processes involve three-phase flow, that is, the simultaneous flow of oil, water, and gas in the reservoir. Practical examples include primary production below bubble point and with movable water, waterfloods in the presence of free gas, gas floods, and water-alternating-gas injection processes. Models of three-phase flow in porous media are also required to describe many problems of environmental interest, such as contamination (and subsequent remediation) of the vadose zone by non-aqueous phase liquids, and geological CO_2 sequestration. In all these cases, reliability of numerical simulation predictions depends critically on the ability to incorporate the heterogeneity present in the system, which in turn leads to simulation models with a very large number of grid blocks. As a result, there is – and there will continue to be in the foreseeable future – need for faster and more robust numerical solution methods.

During the past decade, there has been a renewed interest in streamline-type methods because of their potential for providing fast numerical solutions [27]. The underlying idea is to decouple the three-dimensional transport equations into a set of one-dimensional problems along streamlines. Streamlines are computed from the solution of a properly defined pressure equation. In this way, streamline-type methods exploit the completely different character of the essentially elliptic pressure equation and the essentially hyperbolic system of saturation equations. Streamline and other related methods, however, rely heavily on the efficient solution of the transport equations along one-dimensional domains. In this paper, we propose a front tracking method for solving one-dimensional three-phase flow problems.

The term 'front tracking' usually refers to a family of numerical methods that perform some kind of tracking of shocks and other evolving discontinuities. Most front-tracking schemes consist of a finite-difference scheme coupled with a recipe for detecting and tracking discontinuities. Our method is different in the sense that no finite differences are involved. Instead, the numerical solution is computed by treating all waves as discontinuities. Smooth rarefaction waves are approximated by small discontinuities that violate the entropy condition, whereas shocks and other discontinuities are tracked exactly. The corresponding numerical method comes from a mathematical algorithm [6,22,36] for constructing approximate and *exact* solutions to (systems of) hyperbolic conservation laws of the form

$$u_t + f(u)_x = 0, \qquad u(x,0) = u_0(x). \tag{1}$$

Here $u \in \mathbb{R}^m$ for $m \geqslant 1$, $x \in \mathbb{R}$ and $t \geqslant 0$. The front-tracking construction – which is sometimes called wave front tracking or Dafermos' method – was introduced in its current form as an analytic tool to prove existence for scalar equations [12] and systems of equations [36]. However, the most important application of the method came when it was used as an essential tool in proving uniqueness for systems of conservation laws in one spatial dimension [7,8].

Front tracking, and other closely related constructive methods, has been used by several researchers for numerical computations of discontinuous solutions in one space dimension, and in several space dimensions through a fractional step procedure; see [22] for a complete (historical) overview. The most appealing features of the method are that it is able to resolve discontinuities *exactly*, has no grid dependence, and is unconditionally stable. Depending upon the availability of a fast Riemann solver and the complexity of the wave interactions of the problem, the method can be very efficient compared with conventional finite volume and finite element methods. Furthermore, for scalar equations one can prove that the method has a finite number of steps in infinite time [21]. Somewhat surprisingly, the method has not yet become part of the standard numerical repertoire for conservation laws. The only exception is perhaps within porous media flow, where front-tracking is a key technology in obtaining the high numerical efficiency of the two-phase version of the streamline simulator FrontSim [5] by Schlumberger.

The use of front tracking for the simulation of three-phase flow in porous media has been hindered by the lack of analytical solutions of the corresponding Riemann

problem – a particular case of the Cauchy problem (1) where the initial condition consists in two constant states separated by a single discontinuity [4]. Most previous solutions to the three-phase Riemann problem have been limited to overly simplistic relative permeability functions, in which the relative permeability of each phase is assumed to be a function of its own phase saturation alone [13,14,18,29,33,35,38,39]. When this condition is relaxed, and the relative permeabilities are allowed to depend on all saturations, only generic guidelines for the construction of the solution have typically been provided [16,17]. In a recent paper [25], a complete catalogue of solutions was identified when the relative permeability functions satisfy certain physical conditions. Moreover, efficient algorithms for the evaluation of the solution are given. They are based on a predictor–corrector strategy coupled with a Newton iterative scheme, which yields quadratic convergence. Since the solution to the Cauchy problem typically requires computing a large number of Riemann problems, the availability of a general and highly efficient Riemann solver is essential.

In summary, the key ingredients of the approach presented here are:

(1) decoupling of the three-dimensional equations into a global pressure equation, and a system of one-dimensional saturation equations along streamlines;

(2) solution of the Cauchy problem along each streamline by means of a front tracking algorithm; and

(3) the use of an efficient three-phase Riemann solver as a building block for the front tracking solution.

The outline of the paper is as follows. In section 2, we outline the mathematical model. The solution to the three-phase Riemann problem is discussed in section 3. We describe the wave structure that may arise, and pay particular attention to the role of detached branches of the Hugoniot locus on the global solution structure. In section 4 we describe the front-tracking algorithm used to solve the Cauchy problem, with particular reference to discretization of rarefaction waves, and data reduction. Representative one-dimensional simulations are presented in section 5. Examples 1–3 are Riemann problems, in which the front tracking method is compared against the analytical solution and common finite volume schemes. Example 4 is a more involved test problem modeling water-alternating-gas injection in an oil and gas reservoir. In section 6 we present a three-dimensional three-phase flow simulation, in which the front tracking algorithm is used in combination with a streamline method. These numerical simulations illustrate the potential of this approach for fast and accurate quantitative predictions in real three-dimensional, heterogeneous reservoirs. Finally, in section 7, we gather the main conclusions and anticipate future work.

2. Mathematical model of three-phase flow

Under certain assumptions (see, e.g., [10]) the mathematical model describing three-phase flow in porous media may be expressed in terms of a pressure equation,

and a system of saturation equations. For one-dimensional flow, the system of saturation equations takes the form (after re-scaling of the space variable):

$$u_t + f(u)_x = 0, \tag{2}$$

where $u = (S_w, S_g)$ is the vector of water and gas saturations, and $f = (f_w, f_g)$ is the vector of fractional flow functions. The oil saturation is determined by the algebraic relation $S_o = 1 - S_w - S_g$, which dictates that the fluids fill up the entire pore space. If the effects of miscibility, compressibility, capillarity and gravity are neglected, the fractional flow of phase i is simply:

$$f_i = \frac{\lambda_i}{\lambda_T}, \tag{3}$$

where λ_i is the relative mobility of phase i, and $\lambda_T = \lambda_w + \lambda_g + \lambda_o$ is the total mobility. The relative mobility is defined as:

$$\lambda_i = \frac{k_{ri}}{\mu_i}, \tag{4}$$

where k_{ri} and μ_i are the relative permeability and the dynamic viscosity of phase i, respectively.

The relative permeabilities are normally understood as functions of the fluid saturations alone. It is well known that most relative permeability models used today give rise to elliptic regions, that is, open sets in the saturation space where the system (2) is locally elliptic rather than hyperbolic [3,9,10,15,19,20,26,41,42]. There is an ongoing debate on whether elliptic regions are physical, or simply an unintended consequence of the severe modeling assumptions made in the development of three-phase flow models (see, e.g., [2,23,26,42]). In this paper, we adopt the view that elliptic regions are the result of an incomplete model, and we use relative permeability functions that render the system hyperbolic [26].

3. Solution to the Riemann problem

The Riemann problem is a particular case of the Cauchy problem (1) in which the initial condition is given by piecewise constant data, separated by a single discontinuity:

$$u_0(x) = \begin{cases} u_L & \text{if } x < 0, \\ u_R & \text{if } x \geqslant 0. \end{cases} \tag{5}$$

The state u_L is the 'left' or 'injected' state, and u_R is the 'right' or 'initial' state. Solutions to the Riemann problem (especially analytical solutions) are extremely valuable: they offer insight into the behavior of the system, and they can be used as a building block to obtain solutions for problems with more complex initial conditions.

3.1. Wave structure

Analytical solutions to the Riemann problem of three-phase flow have been studied extensively [13,14,16–18,33,35,39,43]. In a recent paper [25], a complete catalogue of solutions was identified, and efficient algorithms for the computation of the solution were given. The main assumptions used to limit the admissible wave structure are: (1) the system is strictly hyperbolic; and (2) both characteristic fields are nongenuinely nonlinear, and the inflection locus of each field is assumed to be a single curve which corresponds to *maxima* of the eigenvalues. The *inflection locus* of the i-family is the set of states at which the i-characteristic velocity attains a maximum or a minimum value when moving along integral curves of the i-family. We define, for any saturation state u, the quantity

$$V_i(u) := \nabla v_i(u) \cdot r_i(u), \tag{6}$$

where v_i is the i-eigenvalue and r_i is the i-eigenvector of the Jacobian matrix $f'(u)$. With this definition, the i-inflection locus is nothing but the contour $V_i = 0$, which separates convexity regions.

Both conditions mentioned above are natural extensions of the corresponding conditions in the two-phase flow case. Under these assumptions, the solution to the Riemann problem comprises two separated waves, $\mathcal{W}_1$ (slow wave) and $\mathcal{W}_2$ (fast wave), connecting three constant states, u_{L} (left), u_{M} (middle) and u_{R} (right):

$$u_{\mathrm{L}} \xrightarrow{\mathcal{W}_1} u_{\mathrm{M}} \xrightarrow{\mathcal{W}_2} u_{\mathrm{R}}. \tag{7}$$

In general, when the characteristic fields are neither genuinely nonlinear nor linearly degenerate in the sense of Lax [31], each wave may be a composite wave of rarefactions and shocks [32]. However, when the inflection loci are connected manifolds of dimension $n - 1$ (n being the size of the system of equations) where the eigenvalues attain maximum values, each composite wave may only involve a rarefaction followed by a left discontinuity [1]. This important result limits the wave structure of three-phase flow models to only nine admissible combinations of waves, because each of the two waves can only be a single rarefaction $\mathcal{R}$, a single shock $\mathcal{S}$, or a composite rarefaction–shock $\mathcal{RS}$.

Rarefaction curves are described in terms of ordinary differential equations, whereas shock curves are defined by algebraic equations (the Rankine–Hugoniot condition). Efficient algorithms for the computation of individual waves can be obtained based on a Newton iterative scheme in combination with an efficient ODE solver for the rarefaction curves. We use the Runge–Kutta (4,5) pair of Dormand and Prince, see [40]. Algorithms for all solution types can then be devised by piecing together the individual waves using a predictor–corrector strategy, which achieves quadratic convergence in all cases [25]. Such optimal methods for the evaluation of the analytical solution are necessary because typical applications of the front-tracking method require millions of calls to the Riemann solver.

3.2. *Detached branches of shock curves*

The usual construction of the Riemann solution [25] assumes that the wave curves are *local*, that is, that they are continuous curves, which emanate from the left and right states. The intermediate constant state is therefore determined as the intersection of a local 1-wave emanating from u_{L}, and a local 2-wave emanating from u_{R}. It turns out, however, that this construction may lead to globally inadmissible Riemann solutions because the wave speeds are not necessarily monotonically increasing (even if both waves are admissible individually). The reason is that the Hugoniot locus, that is, the set of saturation states that satisfy the Rankine–Hugoniot condition for a given reference state, may present *detached branches*. An example of such behavior is shown in figure 1, where $\mathcal{H}_1$ and $\mathcal{H}_2$ correspond to the slow and fast local branches of the Hugoniot locus, respectively, and $\mathcal{H}_{\mathrm{d}}$ is the detached branch.

Detached branches of the Hugoniot locus are typically present for reference saturation states near the vertex of 100% gas saturation. The presence of detached branches in the saturation space is an indication that the solution may not be constructed in the usual way, by connecting local wave curves emanating from the left and right states. To illustrate the role of detached branches in the construction of admissible solutions, we present the three possible solutions of the Riemann problem with initial state $u_{\mathrm{R}} = (0.05, 0.80)$, and injected state $u_{\mathrm{L}} = (0.8, 0.2)$.

The first tentative solution (figure 2) is obtained by connecting the local 1-wave from u_{L} with the local 2-wave from u_{R}. The solution is in this case of type $\mathcal{R}_1\mathcal{S}_1\mathcal{S}_2$; that is, the slow wave is a rarefaction–shock, and the fast wave is a single shock. The computed shock speeds are such that $\sigma_1 > \sigma_2$ and, therefore, the solution is globally inadmissible. On the right plot of figure 2, we show the saturation profiles of water,

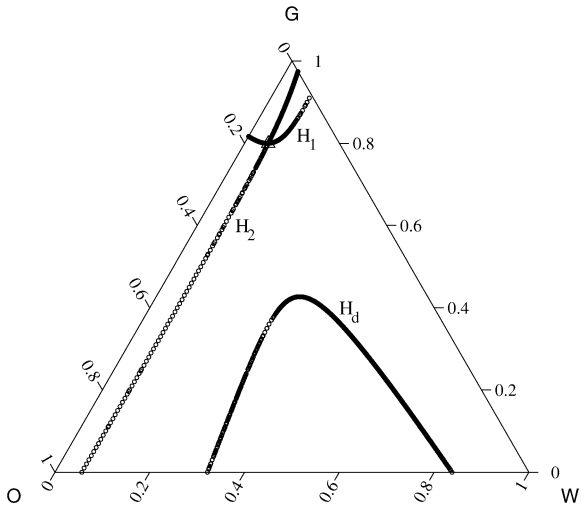

Figure 1. Local and detached branches of the Hugoniot loci for a reference state near the vertex of 100% gas saturation.

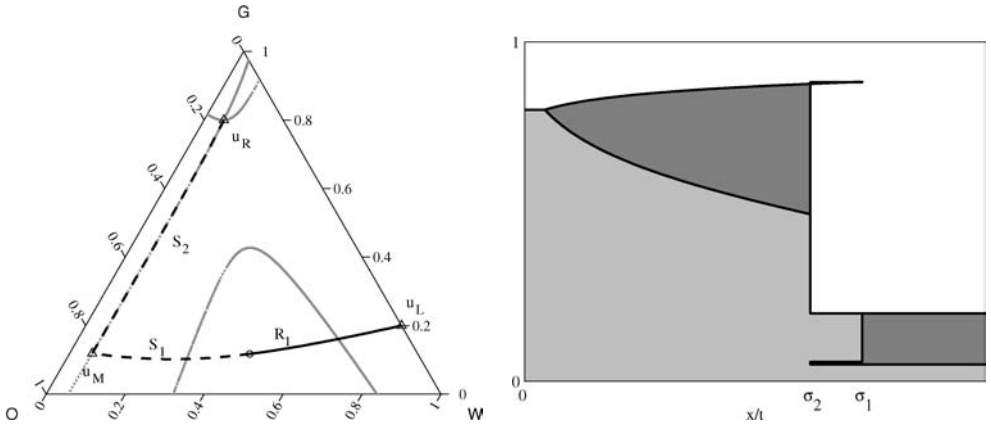

Figure 2. Inadmissible Riemann solution using the local branch of the Hugoniot locus. (a) Saturation path on the ternary diagram; (b) saturation profiles showing a nonincreasing sequence of wave speeds ($\sigma_1 > \sigma_2$).

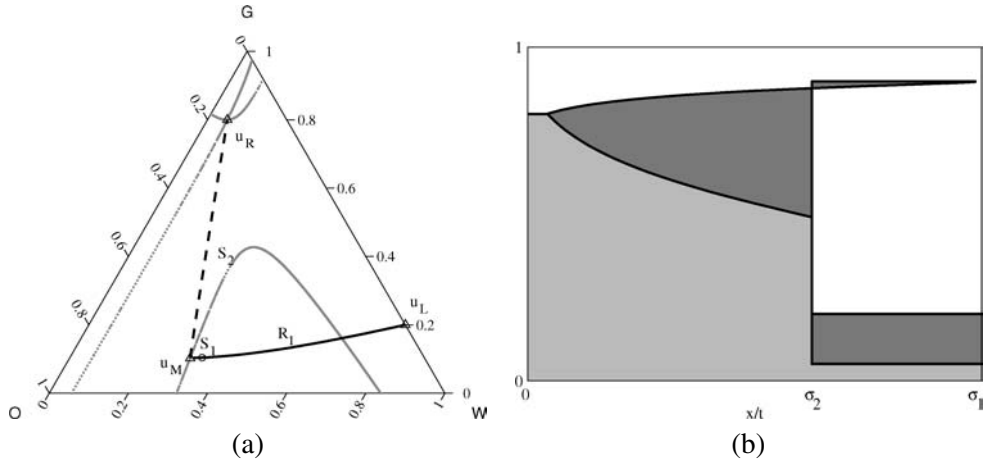

Figure 3. Inadmissible Riemann solution with an intermediate state at the detached branch of the Hugoniot locus. (a) Saturation path on the ternary diagram; (b) saturation profiles showing a nonincreasing sequence of wave speeds ($\sigma_1 > \sigma_2$).

oil, and gas against the similarity variable x/t. The two solid curves correspond to the values of S_w and $1 - S_g$. This is a convenient representation, because it allows to display all three saturations on the same plot: water at the bottom – light gray; gas at the top – in white; and oil in between – in dark gray. The saturation profiles clearly show that the solution is unphysical.

The second tentative solution (figure 3) involves a local 1-wave emanating from u_L, and an intermediate saturation state u_M on the left side of the detached branch. The solution is of type $\mathcal{R}_1\mathcal{S}_1\mathcal{S}_2$ but it is inadmissible because, as before, the wave speeds form a nonincreasing sequence.

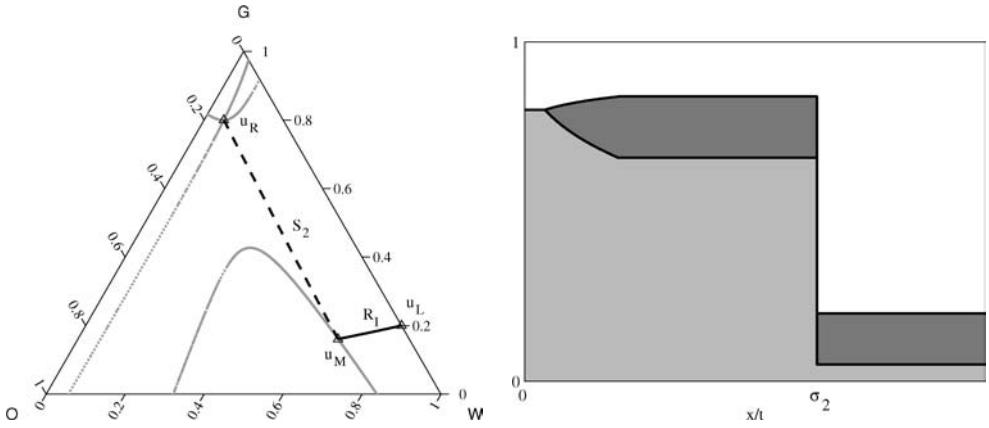

Figure 4. Physically correct Riemann solution, where the right state is reached from an intermediate state at the detached branch of the Hugoniot locus. (a) Saturation path on the ternary diagram; (b) saturation profiles showing a sequence of waves which satisfy the entropy criterion and have increasing speeds.

The third tentative solution (figure 4) connects u_{L} with the intermediate state u_{M} on the right side of the detached branch, which is then connected to u_{R} by a single shock. This is the physically admissible solution because both waves satisfy the e-Lax entropy condition and the wave speeds are monotonically increasing. Indeed, the saturation profiles are uniquely-valued.

The example presented here is representative of the typical behavior of three-phase flow models. Whenever the construction involving local wave curves does not lead to a globally admissible solution, the solution must involve a detached branch. In general, two solutions are then possible, one of which does not satisfy the e-Lax entropy criterion, and the other yields the physically correct Riemann solution. It is important to note that the catalogue of solutions presented in [25] does not change, and that the number of admissible solution types is still nine. Moreover, the predictor–corrector algorithms are also valid and yield quadratic convergence even if the solution involves detached branches. Only the initial guess needs to be judiciously chosen to guarantee that the iterative method converge to the physically correct solution. A more complete study of the role of detached branches on the Riemann solution of three-phase flow models is presented in a separate publication.

3.3. Riemann solver algorithm

The complete algorithm for the determination of the solution to the Riemann problem is presented in algorithm 3.1.

Algorithm 3.1. The Riemann solver algorithm.

1. Given left and right states: u_{L}, u_{R}

2. Set initial guess and trial solution: $u_{\mathrm{M}}^{\mathrm{tr}}$, $\mathcal{W}_1^{\mathrm{tr}} = \mathcal{R}_1$, $\mathcal{W}_2^{\mathrm{tr}} = \mathcal{R}_2$

3. Solve the $\mathcal{W}_1^{\mathrm{tr}}\mathcal{W}_2^{\mathrm{tr}}$ configuration, and update the wave structure:
   $[u_{\mathrm{M}}, \mathcal{W}_1, \mathcal{W}_2] = \mathrm{WaveStruct}(u_{\mathrm{L}}, u_{\mathrm{R}}, u_{\mathrm{M}}^{\mathrm{tr}}, \mathcal{W}_1^{\mathrm{tr}}, \mathcal{W}_2^{\mathrm{tr}})$

4. Check admissibility (increasing wave speeds):
   If $(\sigma_1 > \sigma_2)$ {
   Set new initial guess: u_{M}
   Declare solution invalid: $\mathcal{W}_1^{\mathrm{tr}} = \mathcal{W}_2^{\mathrm{tr}} = 0$ }

5. Check convergence of the algorithm:
   If $\mathcal{W}_1\mathcal{W}_2 = \mathcal{W}_1^{\mathrm{tr}}\mathcal{W}_2^{\mathrm{tr}}$ Stop
   Else Set $\mathcal{W}_1^{\mathrm{tr}}\mathcal{W}_2^{\mathrm{tr}} \leftarrow \mathcal{W}_1\mathcal{W}_2$, $u_{\mathrm{M}}^{\mathrm{tr}} \leftarrow u_{\mathrm{M}}$, Goto 3.

Given the left and right states u_{L} and u_{R}, respectively, the algorithm solves the Riemann problem by determining the intermediate state u_{M} and the wave types $\mathcal{W}_1$ and $\mathcal{W}_2$ joining the three constant states. The algorithm starts by setting an initial guess $u_{\mathrm{M}}^{\mathrm{tr}}$ of the intermediate state, and by assuming a trial solution of type $\mathcal{R}_1\mathcal{R}_2$, that is, a solution consisting in two rarefaction waves. The reason for this choice is that it guarantees that the predicted intermediate saturation state u_{M} will be inside the saturation triangle. The heart of the algorithm is step 3, which involves two actions:

(1) Compute the intermediate state, given a *trial* wave structure $\mathcal{W}_1^{\mathrm{tr}}\mathcal{W}_2^{\mathrm{tr}}$ and an initial guess $u_{\mathrm{M}}^{\mathrm{tr}}$. This step is performed following the algorithms given in [25].

(2) Ascertain what the wave structure of the solution would be *if* the intermediate state were the one just computed. The wave type is inferred separately for each individual wave ($i = 1, 2$). Although this step must be designed carefully to obtain a robust implementation, the concept is quite simple: a valid i-shock must satisfy the Lax entropy criterion; if the shock is not admissible, and the constant states joined by the i-wave are on the same convexity region, the i-wave is a rarefaction; otherwise it is a rarefaction–shock.

Due to the potential presence of detached branches for some saturation states, it is not sufficient to check the admissibility of individual waves. If the solution involves shocks, one must also check that they form an increasing sequence of wave speeds, that is, $\sigma_1 < \sigma_2$. The algorithm terminates if the trial wave structure $\mathcal{W}_1^{\mathrm{tr}}\mathcal{W}_2^{\mathrm{tr}}$ is admissible. Otherwise, both the intermediate state and the wave structure are updated from the computed values. Because rarefaction curves and shock curves typically have similar paths on the saturation space, the intermediate state is usually not very sensitive to the solution type, and the procedure often converges after one iteration.

4. The front-tracking algorithm

Front tracking is an algorithm for constructing exact or approximate solutions to hyperbolic conservation laws of the form

$$u_t + f(u)_x = 0, \qquad u(x,0) = u_0(x).$$

Assume that the initial function $u_0(x)$ is a piecewise constant function so that the Cauchy problem consists of a series of local Riemann problems (5). Each Riemann problem is connected to its nearest neighbors through common constant states. In the previous section we saw how to solve the Riemann problem exactly to produce a similarity solution, which is commonly referred to as the Riemann fan. Each Riemann fan is local in time and space and consists of a set of constant states separated by simple waves. By connecting the local Riemann fans, one obtains a solution that is global in space. Since each simple wave has a finite speed of propagation, the global solution is well-defined up to the time when the first waves from two neighboring Riemann fans interact. If the two interacting waves are discontinuities, the interaction defines a new local Riemann problem and the new global solution can be constructed by inserting the corresponding local Riemann fan, see figure 5. Assume now that all simple waves admitted by the system are discontinuities. This means that all local Riemann problems will produce constant states separated by discontinuities. Then our construction can be repeated to compute the *exact* solution of the Cauchy problem up to an arbitrary desired time level.

If the system admits rarefactions, as is the case for the three-phase model, the above construction cannot be used directly to construct an exact solution. However, an *approximate* solution can be constructed if we approximate each Riemann fan by a step function so that the approximate Riemann fan consists of constant states separated by space–time rays of discontinuities, see figure 6. To this end, we discretize the smooth rarefaction waves by a series of (small) jump discontinuities and keep the shocks (and the linear discontinuities).

We are now in a position to use the algorithm outlined above to construct a global approximate solution (in space and time) in the same way as one builds a scaffolding.

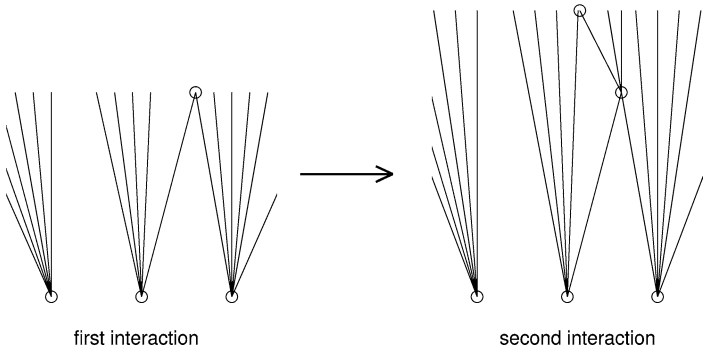

Figure 5. Construction of a global solution by connecting local Riemann fans depicted in the (x,t)-plane.

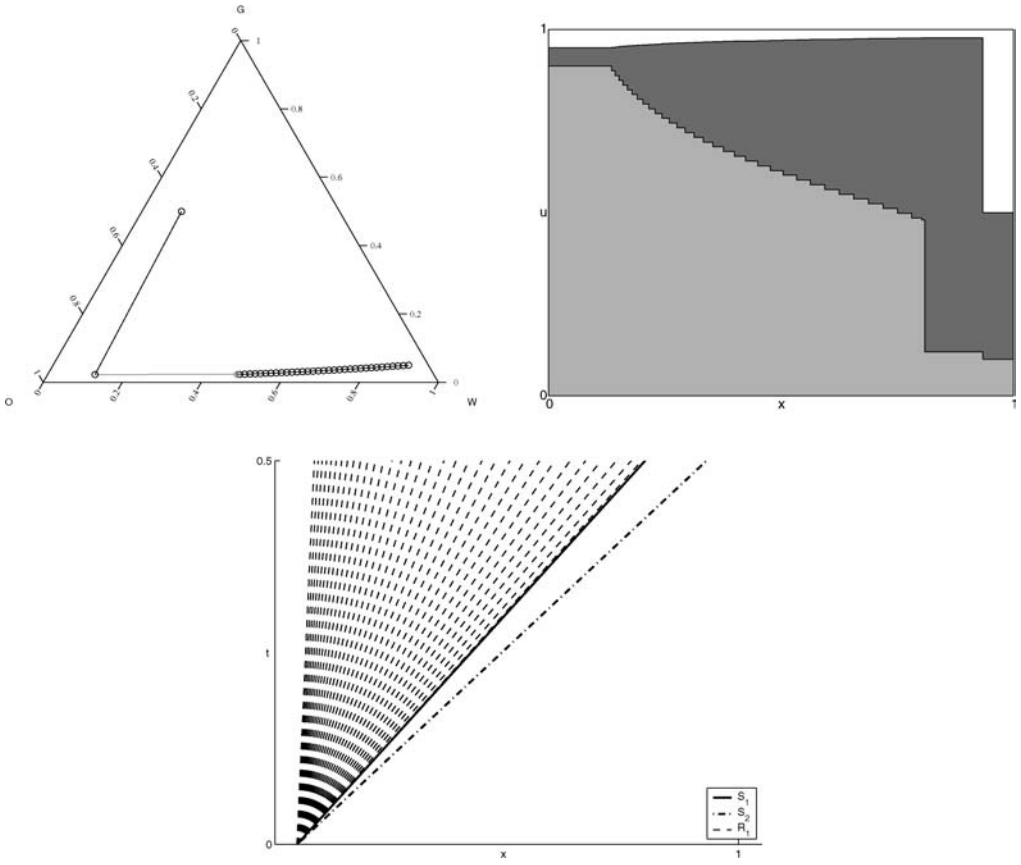

Figure 6. Construction of an approximate Riemann fan: approximation in state space, approximate solution in (x, u)-plane, and fronts in (x, t)-plane.

Start by resolving the initial Riemann problems and connect the local approximate Riemann fans. The result is a set of constant states separated by space–time rays of discontinuity, henceforth referred to as *fronts*. Then, track all fronts until the first two fronts collide, resolve the corresponding Riemann problem, insert the approximate Riemann fan, and so on. This is the front-tracking algorithm, which is outlined in more detail in algorithm 4.1. In the algorithm, the basic data objects are the propagating fronts. Each front object f has an associated left and right state, a point of origin, a propagation speed, and a termination point. To track the fronts, we use two lists, a spatial list F where the fronts are sorted from left to right and a collision list C where front collisions are sorted with respect to collision time in ascending order.

4.1. Approximation of rarefaction waves

We have so far not discussed how to approximate rarefaction waves. There are several ways to do this. One possibility is to discretize each rarefaction wave uniformly

in wave speed. Assume that the integral curve connecting two constant states u_L and u_R is given by $R(\xi)$ for $\xi_L \leqslant \xi \leqslant \xi_R$. Then the constant states approximating the rarefaction are given by $u^i = R(\xi_L + i\delta_\xi)$, where the magnitude of δ_ξ is given by some prescribed parameter and $n\delta_\xi = \xi_R - \xi_L$. In our implementation of the Riemann solver for the three-phase problem, the integral curves are given as either $S_w = R(S_g)$ or $S_g = R(S_w)$. We have therefore chosen a simpler approach, and discretize the rarefactions by sampling uniformly along the integral curves in state space; that is, discretize each rarefaction wave by a set of constant states $\{u^i\}$ such that $|u^i - u^{i-1}| \approx \delta_u$, for some prescribed δ_u.

Since the rarefaction waves are discretized in state space, the wave velocities for each discontinuity must be determined. There are several natural candidates like the characteristic speed of the left or the right state, or the average of the characteristic speeds, see, e.g., [22].

Algorithm 4.1. The front-tracking algorithm.

Construct a piecewise constant initial function $u_0(x) = u_i$
Set $\mathsf{F} = \{\emptyset\}$, $\mathsf{C} = \{\emptyset\}$, and $t = 0$
For $i = 0 : n$
  $\{\mathsf{f}_L, \ldots, \mathsf{f}_R\} = \text{RiemannSolver}(u_i, u_{i+1}, x_{i+1/2}, t)$
  $\mathsf{c} = \text{ComputCollision}(\mathsf{F}, \mathsf{f}_L)$
  $\mathsf{C} = \text{Sort}(\{\mathsf{C}, \mathsf{c}\})$
  $\mathsf{F} = \text{InsertFronts}(\{\mathsf{F}, \{\mathsf{f}_L, \ldots, \mathsf{f}_R\})$
While $(t \leqslant T)$ and $\mathsf{C} \neq \{\emptyset\}$ do
  $(\mathsf{c}, x_c, t_c) = \text{ExtractNextCollision}(\mathsf{C})$
  $\{\mathsf{f}_L, \ldots, \mathsf{f}_R\} = \text{ExtractCollidingFronts}(\mathsf{F}, \mathsf{c})$
  $\{\mathsf{f}_L, \ldots, \mathsf{f}_R\} = \text{RiemannSolver}(\mathsf{f}_L \to u_L, \mathsf{f}_R \to u_R, x_c, t_c)$
  $\{\mathsf{c}_L, \mathsf{c}_R\} = \text{ComputCollision}(\mathsf{F}, \{\mathsf{f}_L, \ldots, \mathsf{f}_R\})$
  $\mathsf{C} = \text{Sort}(\{\mathsf{C}, \mathsf{c}_L, \mathsf{c}_R\})$
  $\mathsf{F} = \text{InsertFronts}(\mathsf{F}, \{\mathsf{f}_L, \ldots, \mathsf{f}_R\})$
endwhile

In our implementation we use the Rankine–Hugoniot wave speed given by the left and right state of each discontinuity, ensuring that each discontinuity in the approximate Riemann fan satisfies the equation in the weak sense, regardless of whether it is admissible or not.

4.2. Data reduction

A potential pitfall of the front-tracking algorithm is that the number of discontinuities in the solution may blow up in finite time for general systems. To prevent this, one must generally use Glimm-type interaction estimates to do some kind of data reduction of weak waves that arise as a result of wave interactions in other families, see [22]. Since the conservation law is continuous in L^1 with respect to its initial data $u_0(x)$, the approximation obtained by replacing u_0 by a piecewise constant function $v(x)$ can be

made arbitrarily good by choosing $v(x)$ appropriately. Similarly, the approximation of the continuous rarefaction waves can be made arbitrarily good by increasing the number of sampling points along the rarefaction waves. If we also design the data reduction carefully, the front-tracking construction will converge to the correct weak solution of (1) in the limit, see [22].

For numerical computations, however, we are only interested in solutions with finite accuracy and not their limit. We can therefore ensure that the front-tracking algorithm terminates in a finite number of steps by removing weak waves (or Riemann problems) below some prescribed tolerance. Moreover, the tracking algorithm can be made more efficient by using an approximate Riemann solver to calculate the interaction of weak waves. Inspired by [30], we propose a general four point strategy for solving the Riemann problem (u_L, u_R) approximately:

(1) If $|u_L - u_R| \leqslant \delta_1$, ignore the Riemann problem.

(2) If $\delta_1 < |u_L - u_R| \leqslant \delta_2$, approximate the Riemann problem by a single discontinuity with shock speed equal the average of the two eigenvalues of the left state.

(3) If $\delta_2 < |u_L - u_R| \leqslant \delta_3$, approximate the Riemann problem by a two-shock solution $\mathcal{S}_1\mathcal{S}_2$. If $\sigma_1 \not\leqslant \sigma_2$, solve the full Riemann problem.

(4) Otherwise solve the full Riemann problem.

The resulting solutions will not be strictly conservative, but the error can be controlled by the parameters δ_u and $(\delta_1, \delta_2, \delta_3)$. Similar data-reductions have been proposed previously [30,37] for other systems of hyperbolic equations.

Let us now look at the motivation for this data reduction. In the second point, we simply ignore the inner structure of the Riemann fan and let the perturbation be passively advected. To determine the wave-speed of the discontinuity one could compute the least squares solution of the associated Rankine–Hugoniot equation. However, this does not ensure a positive wave-speed, and we have therefore chosen to use the average of the eigenvalues. The third point is motivated by the fact that computing rarefaction curves by solving ordinary differential equations is much more expensive than determining the intersection of two Hugoniot loci by solving a nonlinear algebraic equation. If the left and right states are close, the corresponding error will not be large since rarefaction curves and (local) Hugoniot loci coincide at each constant state and deviate only slightly in a small neighborhood. However, the two-shock approximation cannot be used if it does not produce increasing wave-speeds, in which case we go back and solve the Riemann problem exactly.

5. One-dimensional simulations

In the following we will present several simple examples to demonstrate the behavior of the front-tracking algorithm. To this end, we have chosen a simple three-phase

model given by the relative mobility functions

$$\begin{aligned}\lambda_{\mathrm{w}}(S_{\mathrm{w}}) &= \frac{a_{\mathrm{w}}S_{\mathrm{w}} + (1-a_{\mathrm{w}})S_{\mathrm{w}}^2}{\mu_{\mathrm{w}}},\\ \lambda_{\mathrm{g}}(S_{\mathrm{g}}) &= \frac{a_{\mathrm{g}}S_{\mathrm{g}} + (1-a_{\mathrm{g}})S_{\mathrm{g}}^2}{\mu_{\mathrm{g}}},\\ \lambda_{\mathrm{o}}(S_{\mathrm{w}}, S_{\mathrm{g}}) &= \frac{(1-S_{\mathrm{w}}-S_{\mathrm{g}})(1-S_{\mathrm{w}})(1-S_{\mathrm{g}})}{\mu_{\mathrm{o}}},\end{aligned} \tag{8}$$

where $a_{\mathrm{w}} = 0$, $a_{\mathrm{g}} = 0.1$, $\mu_{\mathrm{w}} = 0.35$, $\mu_{\mathrm{g}} = 0.012$, and $\mu_{\mathrm{o}} = 0.8$. With this choice, the system is strictly hyperbolic in the entire saturation triangle, except at the vertex of 100% gas saturation, where the eigenvalues are equal [25].

Two finite-volume schemes

A common way of solving hyperbolic conservation laws like (2) is to use a finite-volume scheme. We will therefore introduce two such schemes that will be used in the next section: the standard first-order upwind scheme and a semi-discrete, second-order, central-upwind scheme [28]. In the following we assume that u_i^n denotes the cell-average function (taken in the componentwise sense)

$$u_i^n = \frac{1}{\Delta x_i}\int_{x_i-(1/2)\Delta x_i}^{x_i+(1/2)\Delta x_i} u\big(x, t^n\big)\,\mathrm{d}x.$$

The upwind scheme has a very simple structure (here $r_i = \Delta t/\Delta x_i$)

$$u_i^{n+1} = u_i^n - r_i\big(f\big(u_i^m\big) - f\big(u_{i-1}^m\big)\big).$$

Among all conservative first-order, three-point schemes, the upwind scheme is the one with the lowest numerical dissipation and can be used componentwise for the three-phase flow equations, since all eigenvalues of this system are positive. Choosing $m = n$ we obtain an explicit scheme, for which we have the stability requirement that $\max_i \nu_2(u_i)r_i \leqslant 1$. A fully implicit scheme is obtained for $m = n+1$.

The central-upwind scheme is a so-called high-resolution scheme. It generally has five points in the stencil and uses a nonlinear reconstruction to guarantee both second-order accuracy and nonoscillatory behavior. In semi-discrete form, the scheme reads

$$\frac{\mathrm{d}}{\mathrm{d}t}u_i(t) = H(u_i, t) = -\frac{1}{\Delta x}\big(F_{i+1/2}(t) - F_{i-1/2}(t)\big).$$

Since all eigenvalues are positive, the numerical flux-functions $F_{i\pm1/2}(t)$ take a particularly simple form

$$F_{i+1/2}(t) = f\left(u_i(t) + \frac{1}{2}u_i'(t)\right),$$

where $u_i'(t)$ is the *reconstructed* discrete slope

$$u_i'(t) = L\big(u_i(t) - u_{i-1}(t), u_{i+1}(t) - u_i(t)\big).$$

For the nonlinear limiter function L we will use the minmod function with $\theta = 1.3$,

$$L(a,b) = \text{minmod}\left(\theta a, \frac{1}{2}(a+b), \theta b\right),$$
$$\text{minmod}\,(a,b,c) = \begin{cases} \min(a,b,c), & a,b,c > 0, \\ \max(a,b,c), & a,b,c < 0, \\ 0, & \text{otherwise.} \end{cases}$$

To integrate the semi-discrete equation we employ a second-order Runge–Kutta scheme based upon combinations of forward-Euler steps

$$u^{(1)} = u^n + \Delta t^n H\big(u^n, t^n\big),$$
$$u^{n+1} = \frac{1}{2}u^n + \frac{1}{2}\big(u^{(1)} + \Delta t^n H\big(u^{(1)}, t^n\big)\big).$$

The stability condition for the central-upwind scheme is $\max_i \nu_2(u_i) r_i \leqslant 1/2$.

Example 1. The first example is a simple Riemann problem at $x = 0.1$ with left state $u_{\mathrm{L}} = (1, 0)$ and right state $u_{\mathrm{R}} = (0, 0.5)$. The example is motivated by water injection in an oil–gas reservoir. The solution is of type $\mathcal{R}_1\mathcal{S}_1\mathcal{S}_2$, as shown in figure 7. Figure 8 shows three approximate solutions obtained with three different choices for the parameter δ_u determining the approximation of rarefaction waves. The $\mathcal{S}_1$ and $\mathcal{S}_2$ shocks are resolved exactly in all three computations and the solution is approximate only along the rarefaction wave. Since rarefactions are approximated in state space and not in wave speed, the step function is uniformly decreasing in S_{w} and nonuniformly

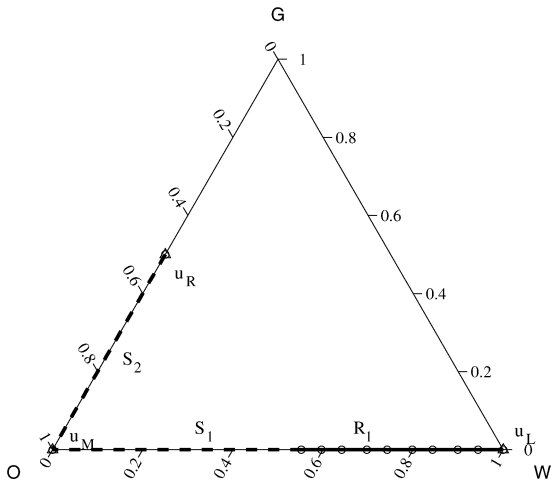

Figure 7. (Example 1) Saturation path of the exact solution and the approximate front-tracking solution with $\delta_u = 0.05$.

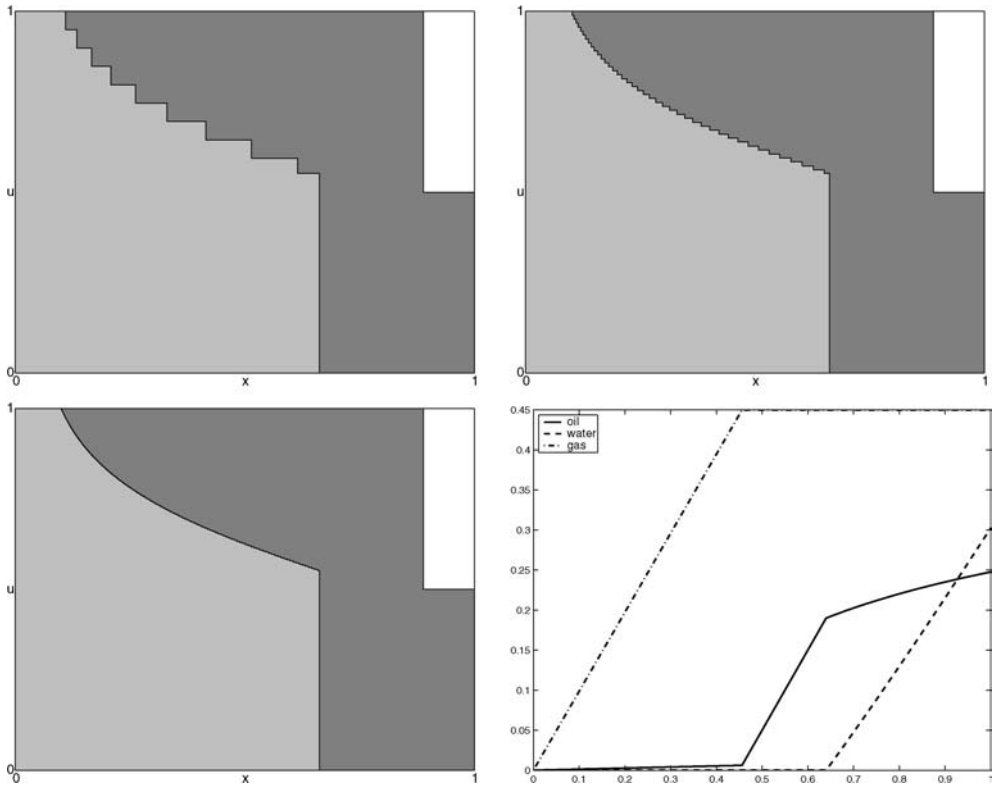

Figure 8. (Example 1) Approximate solutions at time $t = 0.4$ for a water injection in an oil–gas reservoir with $\delta_u = 0.05$, 0.01 and 0.002. The bottom-right plot shows cumulative measured production up to time $t = 1.0$.

increasing in x/t. We observe that the solution converges nicely to the analytical solution as δ_u is decreased.

Figure 8 also shows the cumulative production at the right boundary up to time $t = 1.0$. Initially, the reservoir produces almost only gas. The oil production increases dramatically when the gas has been expelled and decreases again when the water front breaks through.

Example 2. The second example is also a Riemann problem at $x = 0.1$, but now with right state $u_R = (0, 0.75)$. The solution is of type $\mathcal{R}_1\mathcal{S}_2$, where the $\mathcal{S}_2$ wave is on the detached branch of the Hugoniot locus, see figure 9. Figure 10 shows three approximate solutions obtained with three different choices for the parameter δ_u determining the approximation of rarefaction waves.

Given the complexity of the Riemann solver and the front-tracking algorithm, an obvious question to ask is what is gained compared with a finite-volume method. Figure 11 shows a comparison of the front-tracking solution, the upwind scheme, and the central-upwind scheme. The grid size was chosen so that the runtimes of the front-tracker and the upwind scheme were comparable. The runtime of the central-upwind

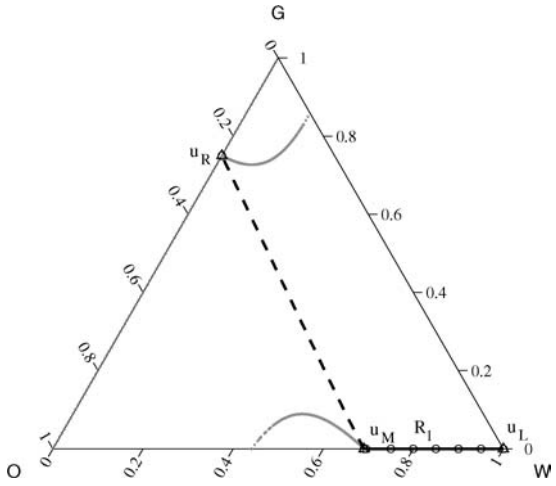

Figure 9. (Example 2) Saturation path of the exact solution and the approximate front-tracking solution with $\delta_u = 0.05$. The $\mathcal{S}_2$ shock involves the detached branch of the Hugoniot locus.

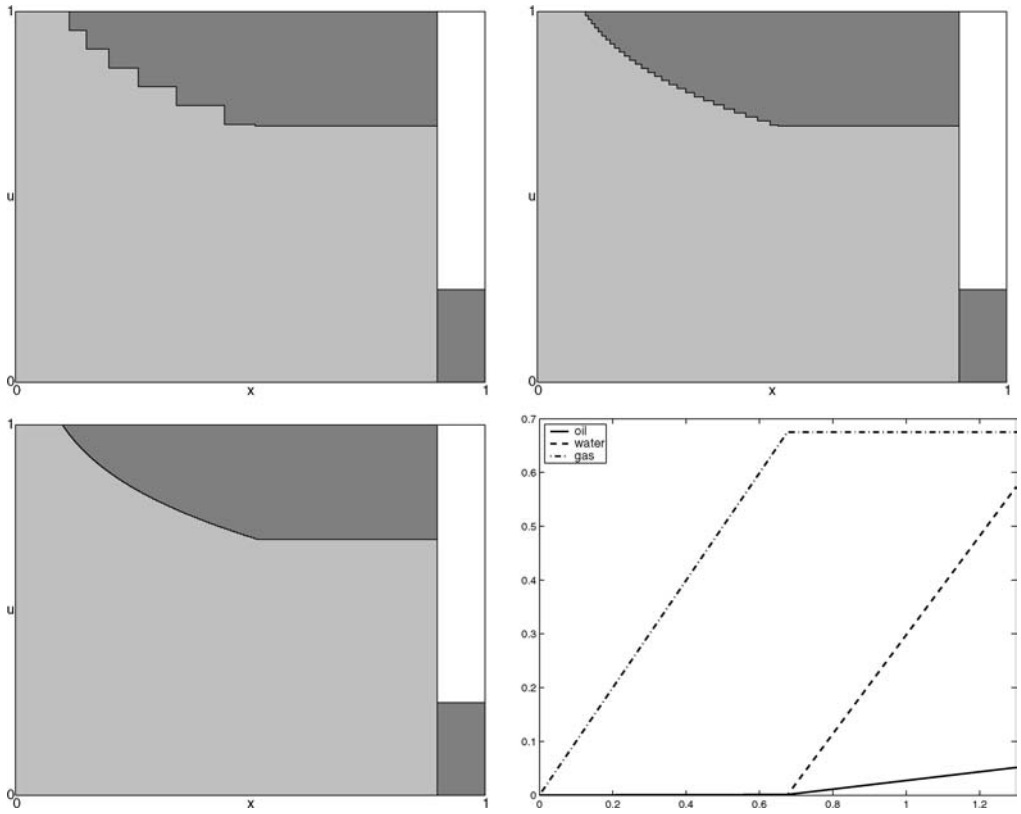

Figure 10. (Example 2) Approximate solutions at time $t = 0.6$ for a solution involving the detached branch of the Hugoniot locus, computed using $\delta_u = 0.05$, 0.01 and 0.002, respectively.

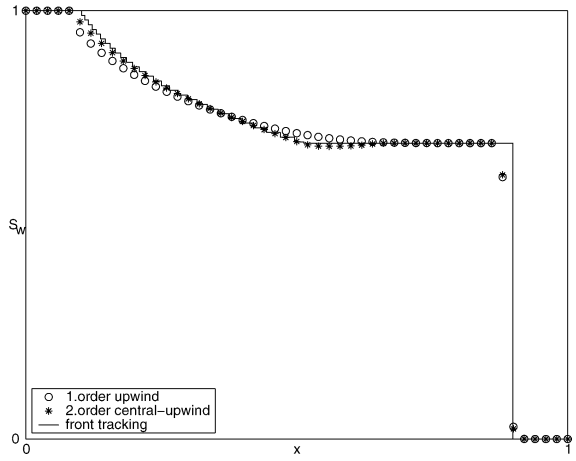

Figure 11. (Example 2) Comparison of the front-tracking solution with $\delta_u = 0.01$ and two finite-volume methods on a grid with $\Delta x = 1/50$.

scheme was a factor 5–6 larger. Whereas the two finite-volume schemes have comparable numerical dissipation at the water front, the smooth rarefaction is resolved better by the second-order scheme. The front-tracking scheme gives exact resolution of the shock and slightly better resolution of the rarefaction wave, but altogether the performance of the three schemes is similar.

Example 3. The third example is also a Riemann problem with $u_{\mathrm{L}} = (0, 0.6)$ and $u_{\mathrm{R}} = (0.4, 0.05)$. The wave structure is $\mathcal{R}_1\mathcal{S}_1\mathcal{R}_2$, where the $\mathcal{S}_1$ wave is very weak with $|u_l - u_r| = 0.0039$. Figure 12 compares approximate solutions at $t = 0.1$ obtained by the two finite-difference schemes on a grid with 50 cells with the exact solution. As expected, the ternary diagram shows that the two finite-volume schemes do not resolve the structure of the $\mathcal{W}_1$ wave on this coarse grid. To resolve the structure, one must in fact increase the number of grid points by at least two orders of magnitude, as can be seen in figure 13, where we have zoomed in on the solution around the $\mathcal{W}_1$ wave. Front-tracking, on the other hand, gives a fair approximation to the $\mathcal{W}_1$ wave even with $\delta_u = 0.05$.

Example 4. As a fourth example, we model a simplified water-alternating-gas (WAG) process, in which the injected conditions vary in time. We consider a linear reservoir with initial saturations of 20% gas and 80% oil, so that $u_{\mathrm{R}} = (0, 0.2)$. The process starts by injecting pure water, which defines a Riemann problem with $u_{\mathrm{L}} = (1, 0)$. At time $t = 0.1$, the injected state is changed to $u_{\mathrm{L}} = (0.01, 0.99)$, corresponding to almost 100% gas injection. Subsequent cycles of water and gas injection are established, with each injection phase lasting for a period $\Delta t = 0.1$.

Because of the stepwise change in the left boundary condition, the solution is no longer a single Riemann fan. Figure 14 shows the fronts in the (x, t)-plane for a very coarse approximation $\delta_u = 0.05$. The total number of Riemann problems solved for this simulation was approximately 26 000. The initial wave structure consists of a fast

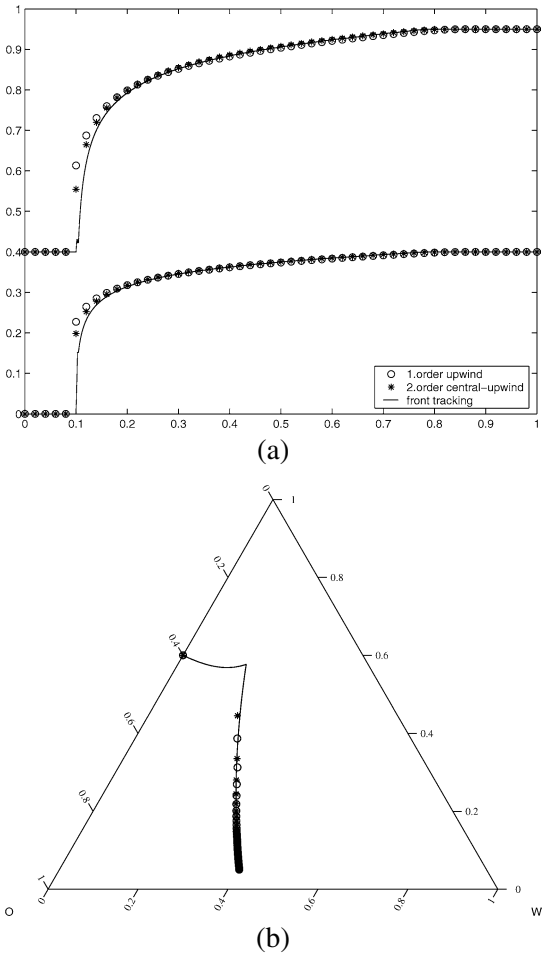

Figure 12. (Example 3) Comparison of the front-tracking solution with $\delta_u = 0.001$ and two finite-volume methods on a grid with $\Delta x = 1/50$; (a) plot shows solutions in the (x, u)-plane and (b) plot shows solutions in the ternary diagram.

2-shock that displaces the initial oil–gas mixture by pure oil, followed by a rarefaction–shock in the first family displacing oil by water (as in the classical two-phase Buckley–Leverett displacement). When gas is injected at time $t = 0.1$, the injected gas gives a fast rarefaction–shock in the second family that travels unperturbed through the injected water. As the gas front passes, the injected water slows down, as can be seen from the kink in the waves of the first family. The injected gas front overtakes the gas front induced by the first water injection cycle and the oil bank reaches the production well at $t \approx 0.564$.

In figure 15 we plot the saturation profiles at times $t = 0.1$, 0.2, 0.5, 1.5 and $t = 2$, calculated with the front-tracking method and the standard first-order upwind method. In the front-tracking solution, we used $\delta_u = 0.005$ for an accurate sampling of the rarefaction waves. The front-tracking method requires in this case the solution of

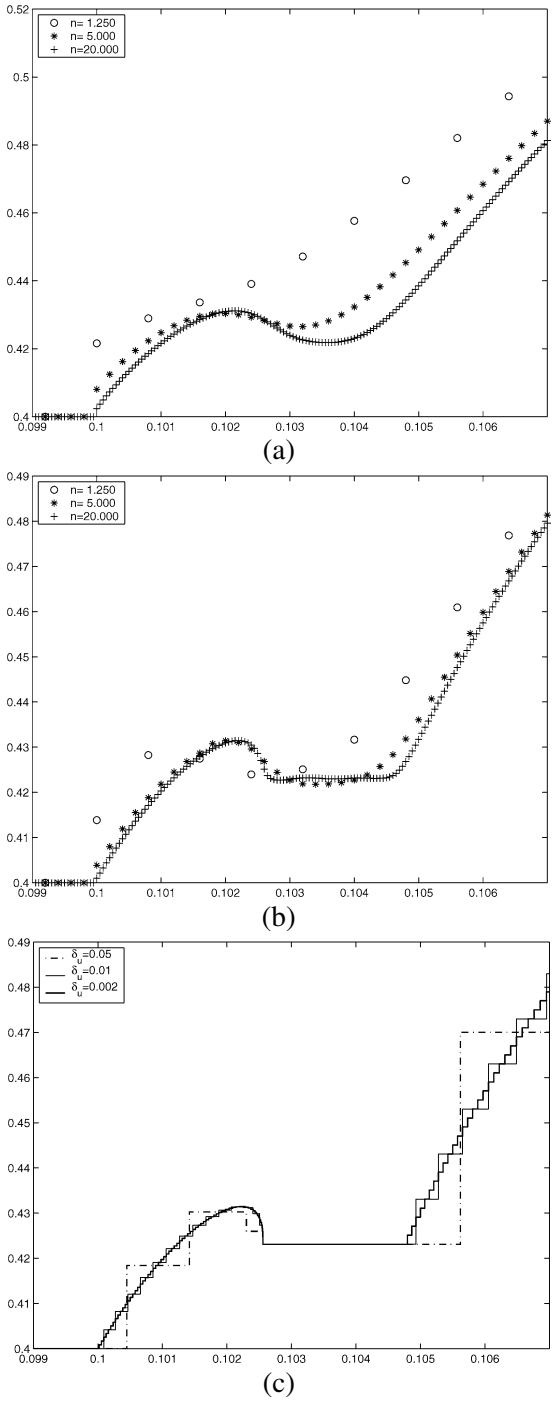

Figure 13. (Example 3) Plot of $1 - S_g$ zoomed in around the $\mathcal{W}_1$ wave. Approximate solutions computed by first-order upwind (a) and second-order central-upwind (b) on a grid with n cells, compared with front-tracking (c).

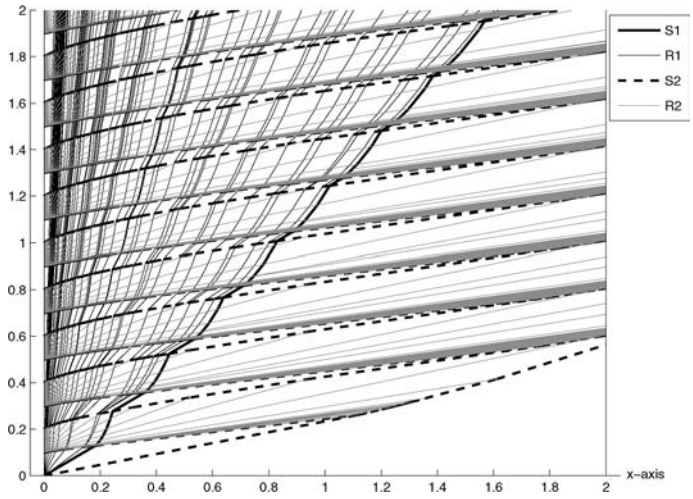

Figure 14. (Example 4) Fronts in the (x, t)-plane for the simplified WAG process, using $\delta_u = 0.05$.

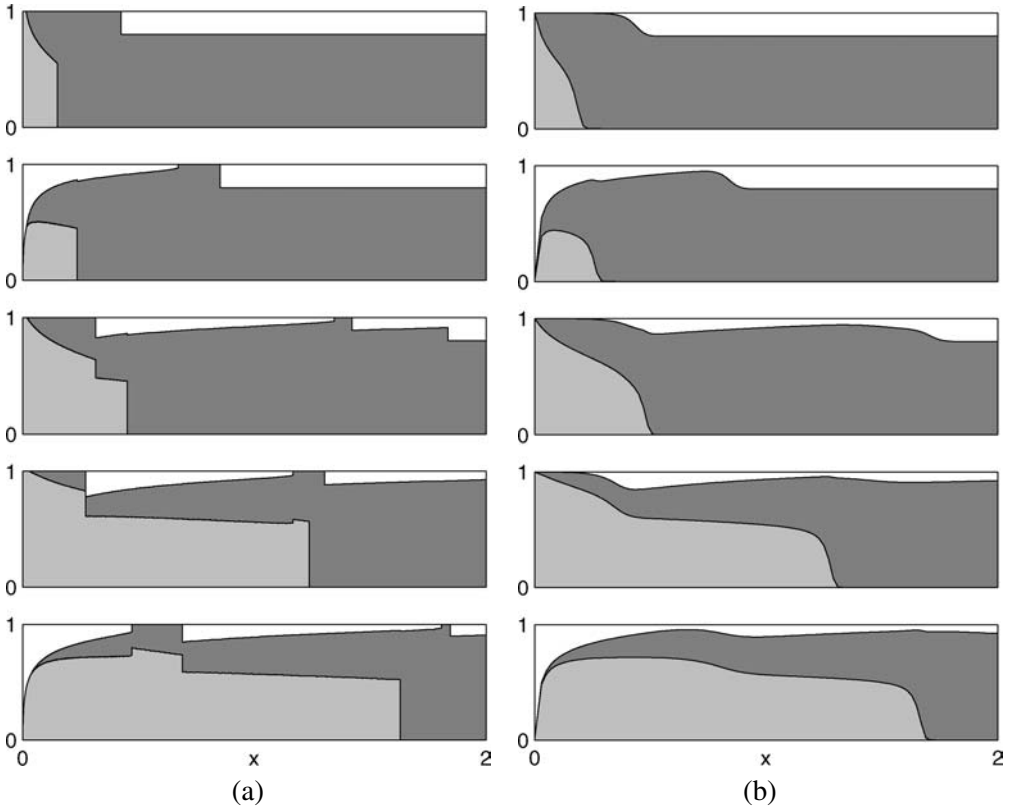

Figure 15. (Example 4) Saturation profiles for the one-dimensional WAG process at $t = 0.1$ (top), 0.2, 0.5, 1.5 and $t = 2$ (bottom), calculated by: the front-tracking using $\delta_u = 0.005$ (a), and the first-order upwind method with 100 grid cells (b).

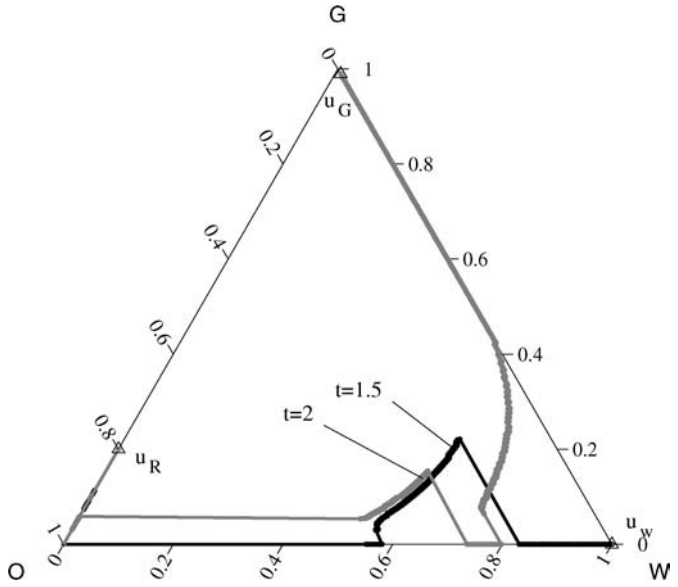

Figure 16. (Example 4) Saturation path at two different times.

about 1.5 million Riemann problems. The finite difference solution was computed with 100 grid cells, and a fully implicit time stepping procedure. We employed a constant time step $\Delta t = 0.005$, which corresponds to a Courant number $Co = \sigma_2 \Delta t / \Delta x \approx 1$. With this discretization, the computational effort of both methods is comparable. It is apparent that the front-tracking method gives a very accurate resolution of moving fronts, while the solution obtained with the finite difference upwind method is greatly affected by numerical diffusion.

Additional insight into the behavior of the solution can be gained by plotting the solution as a saturation path on the ternary diagram. Figure 16 shows the solution at times $t = 1.5$ (end of a water injection cycle) and $t = 2$ (end of a gas injection cycle). Each path must necessarily start at the saturation state of the injected conditions. Sharp changes in the saturation path indicate strong shocks, which move across the domain by the action of the injected fluids.

The cumulative production curves are shown in figure 17 up to time $t = 4$. Until $t \approx 0.564$, the reservoir produces mostly gas. At that time, the leading oil bank reaches the right boundary, and the oil production increases significantly. The oil production rate drops dramatically after $t \approx 2.5$, which is when the injected water breaks through.

Example 5. In the fifth example we look at the effects of using the data reduction introduced in section 4.2. To this end, we simplify the WAG injection discussed above by increasing the injection phases to a period $\Delta t = 0.5$. We start by comparing two simulations using $\delta_u = 0.05$; a simulation without data reduction and a simulation where all Riemann problems with strength below $\delta_3 = 0.2$ are treated as $\mathcal{S}_1\mathcal{S}_2$ waves. Whereas

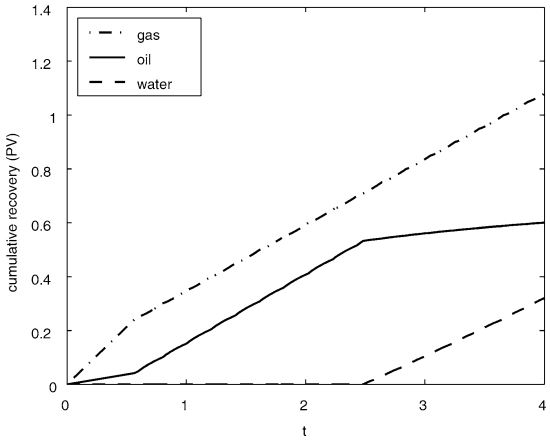

Figure 17. (Example 4) Production curves.

the full simulation required 787 Riemann solves, the second simulation required only 369 Riemann solves, out of which 325 were shock–shock approximations.

Figure 18 shows fronts in the (x, t)-plane for the two simulations. The first Riemann problem at $(0, 0)$ gives a $\mathcal{R}_1\mathcal{S}_1\mathcal{S}_2$ solution. When the injection is changed at $t = 0.5$, this gives a Riemann problem at $(0, 0.5)$ with a $\mathcal{R}_2\mathcal{S}_2$ solution. Almost immediately afterwards, the fronts in the $\mathcal{R}_1$-wave emanating from $(0, 0)$ will start interacting with the fronts in the $\mathcal{R}_2$-wave emanating from $(0, 0.5)$. Since we use a rather large threshold value $\delta_3 = 0.2$, each of these waves are approximated by a $\mathcal{S}_1\mathcal{S}_2$ solution. Later on, these $\mathcal{S}_2$-fronts interact with the $\mathcal{S}_1$-front emanating from $(0, 0)$. Since the strength of these interactions are not below the threshold, the corresponding Riemann problems will be solved exactly and correctly produce a $\mathcal{S}_1\mathcal{R}_2$ pair of fronts, as for the case without data reduction. Figure 19(a) compares the saturation profiles at $t = 2.0$ for the two approximate solutions. Although the approximations in (x, t)-space are quite different in terms of the waves used, the saturation profiles almost coincide.

Figure 19(b) shows a comparison of a full simulation for $\delta_u = 0.005$ and a simulation with data reduction given by $\delta_3 = 0.2$ and $\delta_2 = 0.01$. The full simulation required 73 360 Riemann solves, whereas the data-reduced simulation required only 7 475 Riemann solves, out of which 212 were full solves, 6 991 were $\mathcal{S}_1\mathcal{S}_2$ approximations, and 272 were approximation by a single wave. Whereas the number of Riemann solves were reduced by a factor 10, the runtime was reduced by a factor 40, owing to the faster computation of Hugoniot loci compared with rarefaction curves.

Computational efficiency

One important question that remains to be discussed is how the computational efficiency of the front-tracking method compares with that of standard finite-difference schemes like the first-order upwind scheme. Two simple comparisons were given in

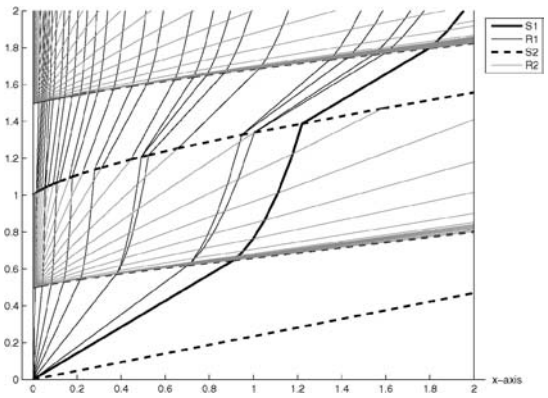

(a)

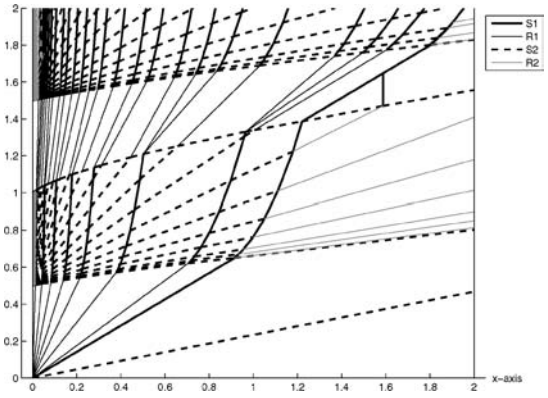

(b)

Figure 18. (Example 5) Fronts in the (x, t)-plane for a WAG process computed with $\delta_u = 0.05$ and no data reduction (a) and with data reduction given by $\delta_3 = 0.2$ (b).

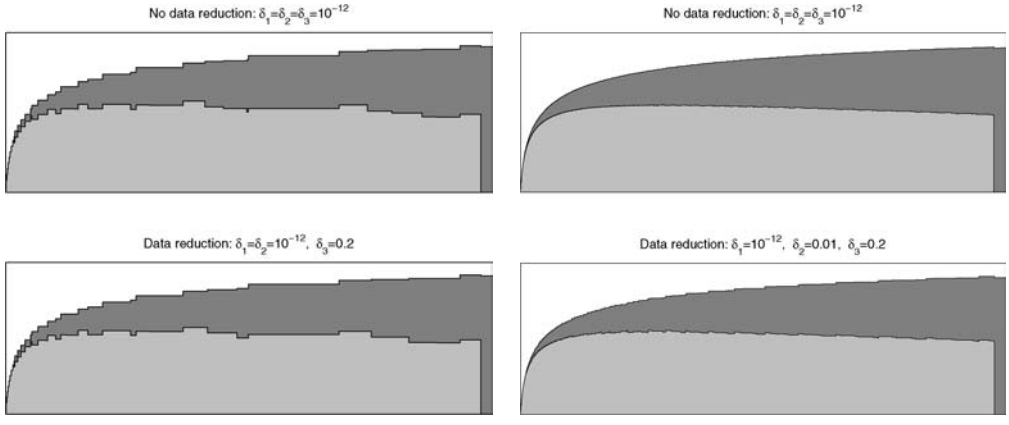

(a) (b)

Figure 19. (Example 5) Saturation profiles at $t = 2.0$ computed with $\delta_u = 0.05$ (a) and $\delta_u = 0.005$ (b).

examples 2 and 4 and indicated that the front-tracking method (even without data reduction) delivers superior accuracy compared with finite-difference methods for a given computational cost. However, making a general comparison is more difficult, since the factors determining the runtime are not the same for finite-difference schemes and the front-tracking method. The runtime of a finite-difference scheme is basically determined by the number of grid-cells and the number of time-steps. The runtime of the front-tracking method is determined by the complexity of the wave interactions in the problem and the number of discontinuities used to approximate the rarefactions. The method will therefore be most efficient for problems involving few wave interactions or cases that would require highly irregular grids in a finite difference methods (as discussed, for instance, in the next section).

6. Three-phase streamline simulation

An interesting application of the front-tracking method for three-phase flow is in combination with streamlines to simulate multidimensional displacement scenarios. In a streamline simulation, the pressure and the transport equations are decoupled and solved sequentially. A streamline is defined as the flow path traced out by a neutral particle being passively advected by a flow field so that the velocity field v is tangential to the streamline at every point. The streamlines are parametrized by the so-called *time-of-flight* $\tau = \tau(x)$ that measures the time it takes for a passive particle released at the boundary (i.e., an injector) at time zero to reach a point x in physical space. The time-of-flight can be computed by integrating along individual streamlines Ψ

$$\tau(s) = \int_0^s \frac{(\phi \circ \Psi)(\xi)}{|(v \circ \Psi)(\xi)|}\, \mathrm{d}\xi,$$

where v is the total Darcy velocity and ϕ is the porosity. In the simulator, the streamlines are traced from cell to cell using an analytic method due to Pollock [34]. For incompressible flow, all streamlines will start in an injector and end in a producer. In the fluid transport, each streamline is treated as an isolated flow system described by the one-dimensional hyperbolic system (in the case of no gravity)

$$u_t + f(u)_\tau = 0, \qquad u(\tau, 0) = u_0(\tau). \tag{9}$$

In a streamline method, the saturations are advanced forward in time by solving (9), here by using the front-tracking method. At the end of the transport step, the saturations are projected back onto the background grid, the fluid mobilities are updated, and the pressure recomputed.

The initial data $u_0(\tau)$ are obtained by mapping saturations from a grid in physical space to a time-of-flight grid along each streamline, where the size of the grid-cells in τ is given by the traversal times of the grid-cells in physical space. The resulting grids are highly irregular, with small grid-cells close to injectors and producers and large

cells in the middle of the reservoir. For streamline simulators using finite-differences to solve (9), one therefore has to use an adaptive formulation and/or resample the initial data on a more regular grid. The front-tracking method, on the other hand, has no difficulty coping with highly-irregular grids, since these are only used to set up the initial Riemann problems. This is one of the definite advantages of the front-tracking method.

For a full three-dimensional simulation, the saturation step typically involves several thousand streamlines, resulting in a very large number of calls to the Riemann solver. The Riemann solver must therefore be highly efficient. In the current three-phase solver, the most expensive part is the calculation of rarefactions and rarefaction–shocks, because they involve constrained integration of ordinary differential equations. To increase the speed significantly, we will therefore use the simple *adaptive* Riemann solver introduced in section 4.2, for which the wave structure of strong Riemann problems is resolved exactly, whereas weak Riemann problems are ignored or approximated by a (possibly inadmissible) two-shock solution.

We consider a synthetic, full three-dimensional reservoir model consisting of a five spot well configuration (one injection well at the center and four production wells at the corners) in a highly heterogeneous, shallow-marine Tarbert formation. The heterogeneity model is a subsample of the recent 10th SPE comparative solution project [11] on a $30 \times 110 \times 15$ grid. The field has large (but smooth) permeability variations: 6 orders of magnitude in the horizontal direction and 10 orders in the vertical direction, see figure 20. The porosity is strongly correlated to the permeability.

For simplicity, we neglect gravity and assume incompressible flow. The three-phase model is as given in the previous section. The initial saturation is $(S_w, S_g) =$

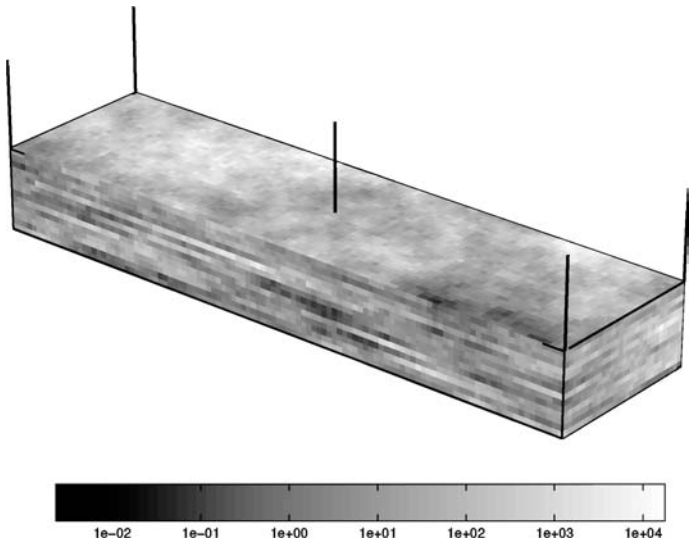

Figure 20. Logarithm of horizontal permeability and well configuration for the Tarbert formation.

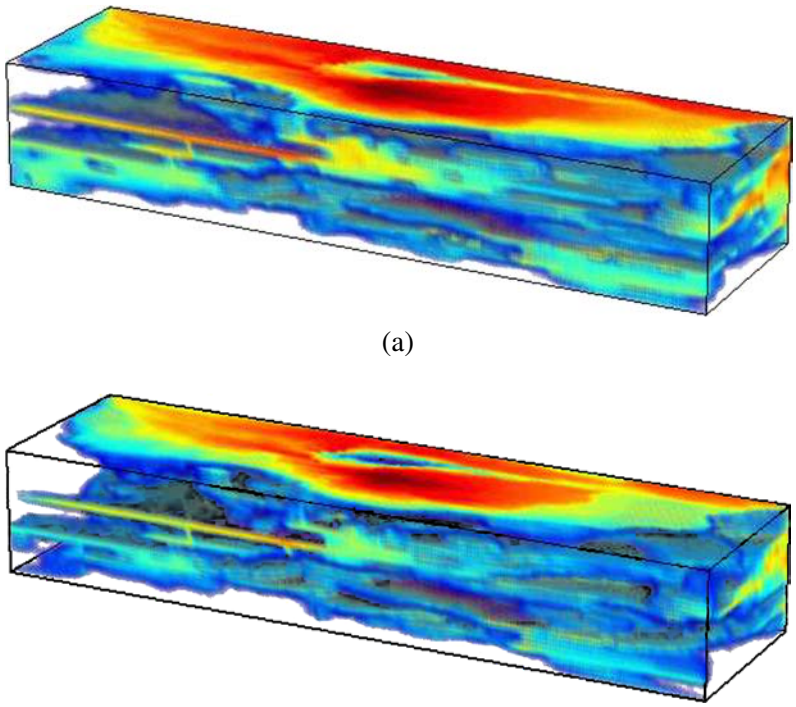

(a)

(b)

Figure 21. Water saturation after 2 000 days of production with constant water injection (a) and a WAG cycle (b).

$(0.0, 0.2)$. We consider 2 000 days of production by two different scenarios: (i) injection of pure water, i.e., $(S_w, S_g) = (1.0, 0.0)$; and (ii) a WAG cycle where the injected fluid composition is changed between pure water and $(S_w, S_g) = (0.05, 0.95)$ every 200th day, starting at day 400.

Figure 21 shows the water saturation after 2 000 days of production for the two scenarios, computed using 10 000 streamlines and $\delta_u = 0.025$ in the approximation of rarefaction waves. The WAG simulation involved 632 million calls to the Riemann solver, out of which 617 million satisfied $|u_L - u_R| \leqslant 0.2$ and were approximated by a two-shock solution.

Figure 22 shows a comparison of the production rates for oil, gas and water obtained by our streamline solver and Eclipse, which is a industry-standard finite-difference simulator. Whereas Eclipse uses an implicit formulation with adaptive stepsize control, our solver uses a fractional step formulation with no stepsize control. To assess the error in the operator splitting, we present results obtained with different step sizes between days 400 and 2 000. Given the fundamentally different nature of the Eclipse and the streamline method, the production curves are in remarkable agreement.

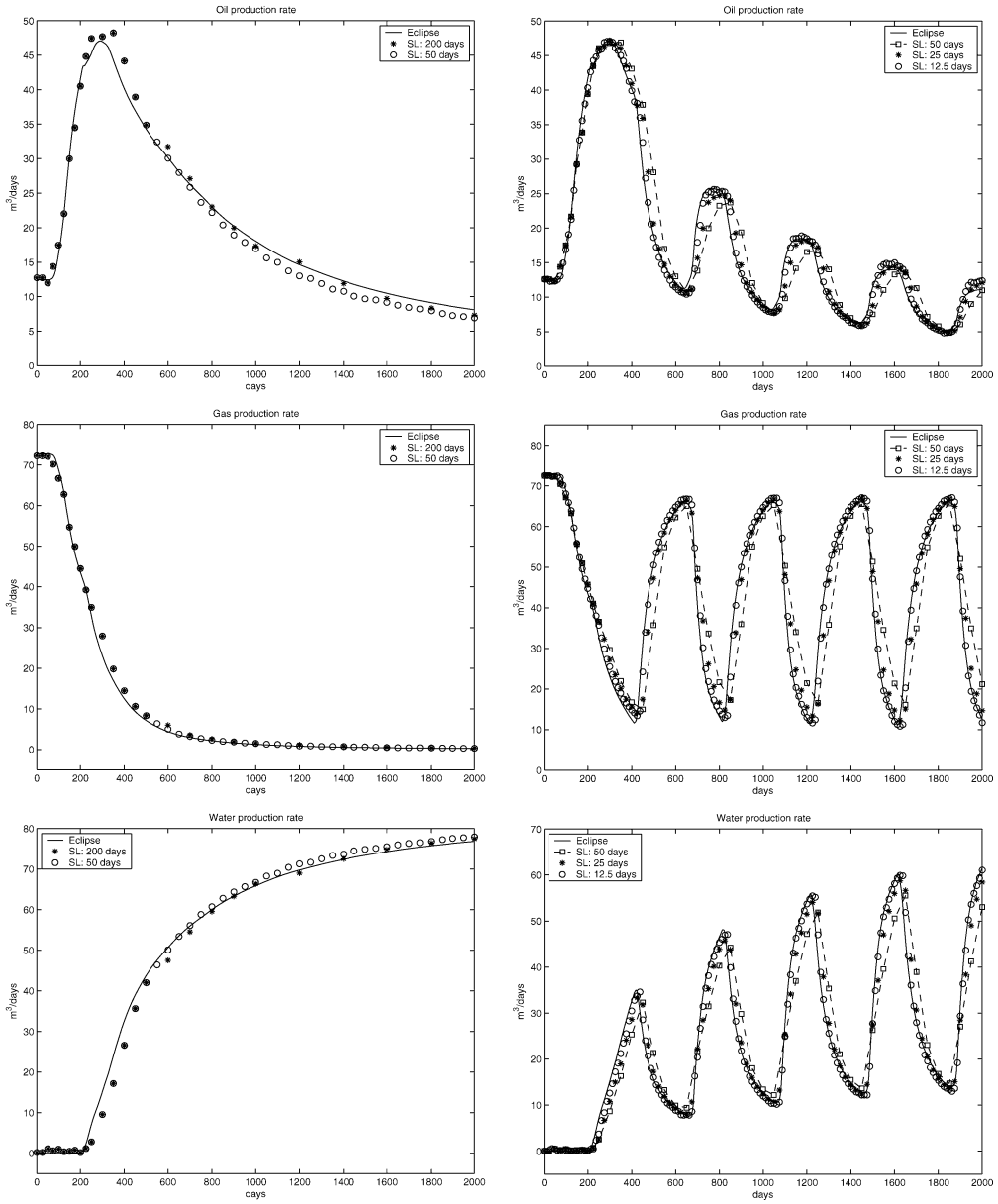

(a) (b)

Figure 22. Oil, gas, and water rates for water injection (a) and the WAG cycle (b).

Worth noting also is that the streamline simulations are significantly faster. On a dual 2.0 MHz Pentium PC, the Eclipse simulations took 1 hr 22 min for the water injection, and 8 hr 20 min for the WAG cycle. The timings for the streamline simulator were 50 minutes for the water injection with stepsize 200 days, and 2 hr 13 min for the WAG cycle using stepsize 25 days.

7. Conclusions

In this paper we have presented a front-tracking method for the numerical solution of three-phase porous media flow. The method is developed for constructing very accurate (even exact) solutions to one-dimensional problems with general initial and boundary data. The solution is approximated by a piecewise constant function, and the evolution of discontinuities is resolved by using the analytical solution to the Riemann problem. It is the use of the *exact* analytical solution, together with an appropriate algorithm to simplify the wave structure for Riemann problems of small amplitude, what makes the front-tracking technique very attractive as a computational method. We have illustrated the performance of the method with several one-dimensional simulations, and compared the results with two finite-volume schemes. The main advantage of the front-tracking method is that strong shocks are resolved exactly (both in amplitude and speed).

An important practical application of the front-tracking algorithm arises in the context of streamline simulation. Streamline methods decouple the three-dimensional problem into a set of one-dimensional problems along streamlines, which can then be solved by means of the front-tracking method. In this paper, we have shown the efficacy of the proposed approach for the simulation of a complex, highly heterogeneous, three-dimensional reservoir model adapted from the 10th SPE comparison solution project.

The integration of analytical Riemann solvers, the front-tracking method, and streamline tracing, offers the potential for fast and accurate prediction of three-phase flows in real reservoirs. This technology becomes particularly relevant for screening purposes and for risk assessment, which require the simulation of a large number of scenarios.

The formalism presented here may be extended in several ways. The Riemann solver was limited to three-phase immiscible, incompressible flow, and we are currently working on its extension to account for miscibility effects [24]. Other physical processes, such as gravity, capillarity, and compressibility, may also be incorporated into the streamline simulator.

Acknowledgements

R.J. gratefully acknowledges financial support from the industrial affiliates of the Stanford University Petroleum Research Institute for Numerical Simulation (SUPRI-B) and Gas Injection (SUPRI-C). K.-A.L. gratefully acknowledges financial support from the Research Council of Norway under grant number 158908/I30.

References

[1] F. Ancona and A. Marson, A note on the Riemann problem for general $n \times n$ conservation laws, J. Math. Anal. Appl. 260 (2001) 279–293.

[2] A.V. Azevedo, D. Marchesin, B. Plohr and K. Zumbrun, Capillary instability in models for three-phase flow, Z. Angew. Math. Phys. 53 (2002) 713–746.

[3] J.B. Bell, J.A. Trangenstein and G.R. Shubin, Conservation laws of mixed type describing three-phase flow in porous media, SIAM J. Appl. Math. 46(6) (1986) 1000–1017.
[4] I. Berre, H.K. Dahle, K.H. Karlsen and H.F. Nordhaug, A streamline front tracking method for two- and three-phase flow including capillary forces, in: *Fluid Flow and Transport in Porous Media: Mathematical and Numerical Treatment*, eds. Z. Chen and R.E. Ewing, Contemporary Mathematics, Vol. 295 (Amer. Math. Soc., Providence, RI, 2002) pp. 49–61.
[5] F. Bratvedt, K. Bratvedt, C.F. Buchholz, T. Gimse, H. Holden, L. Holden and N.H. Risebro, Frontline and Frontsim, two full scale, two-phase, black oil reservoir simulators based on front tracking, Surveys Math. Indust. 3 (1993) 185–215.
[6] A. Bressan, Global solutions of systems of conservation laws by wave-front tracking, J. Math. Anal. Appl. 170 (1992) 414–432.
[7] A. Bressan, G. Crasta and B. Piccoli, Well-posedness of the Cauchy problem for $n \times n$ systems of conservation laws, Mem. Amer. Math. Soc. 694 (2000) 1–134.
[8] A. Bressan and P. LeFloch, Uniqueness of weak solutions to systems of conservation laws, Arch. Rational Mech. Anal. 140(4) (1997) 301–317.
[9] I.A. Charny, *Subterranean Hydro-Gas Dynamics* (Gostoptekhizdat, Moscow, 1963) (in Russian).
[10] G. Chavent and J. Jaffré, *Mathematical Models and Finite Elements for Reservoir Simulation* (Elsevier/North-Holland, Amsterdam, 1986).
[11] M.A. Christie and M.J. Blunt, Tenth SPE comparative solution project: A comparison of upscaling techniques, SPE Reserv. Eval. Engrg. 4(4) (2001) 308–317; url: www.spe.org/csp.
[12] C. Dafermos, Polygonal approximations of solutions of the initial value problem for a conservation law, J. Math. Anal. Appl. 38 (1972) 33–41.
[13] A.H. Falls and W.M. Schulte, Theory of three component, three phase displacement in porous media, SPE Reserv. Engrg. 7(3) (1992) 377–384.
[14] A.H. Falls and W.M. Schulte, Features of three component, three phase displacement in porous media, SPE Reserv. Engrg. 7(4) (1992) 426–432.
[15] F.J. Fayers, Extension of Stone's method I and conditions for real characteristics in three-phase flow, in: *SPE Annual Technical Conf. and Exhibition*, Dallas, TX (SPE 16965) (27–30 September 1987).
[16] R.E. Guzmán and F.J. Fayers, Mathematical properties of three-phase flow equations, Soc. Pet. Engrg. J. 2(3) (1997) 291–300.
[17] R.E. Guzmán and F.J. Fayers, Solution to the three-phase Buckley–Leverett problem, Soc. Pet. Engrg. J. 2(3) (1997) 301–311.
[18] F.G. Helfferich, Theory of multicomponent, multiphase displacement in porous media, Soc. Pet. Engrg. J. 21(1) (1981) 51–62.
[19] P.J. Hicks Jr. and A.S. Grader, Simulation of three-phase displacement experiments, Transp. Porous Media 24 (1996) 221–245.
[20] L. Holden, On the strict hyperbolicity of the Buckley–Leverett equations for three-phase flow in a porous medium, SIAM J. Appl. Math. 50(3) (1990) 667–682.
[21] H. Holden, L. Holden and R. Høegh-Krohn, A numerical method for first order nonlinear scalar conservation laws in one-dimension, Comput. Math. Appl. 15(6–8) (1988) 595–602.
[22] H. Holden and N.H. Risebro, *Front Tracking for Hyperbolic Conservation Laws* (Springer, New York, 2002).
[23] M.D. Jackson and M.J. Blunt, Elliptic regions and stable solutions for three-phase flow in porous media, Transp. Porous Media 48 (2002) 249–269.
[24] R. Juanes and K.-A. Lie, A front-tracking method for efficient simulation of miscible gas injection processes, in: *SPE Reservoir Simulation Symposium*, Houston, TX (SPE 93298) (January 31–February 2 2005).
[25] R. Juanes and T.W. Patzek, Analytical solution to the Riemann problem of three-phase flow in porous media, Transp. Porous Media 55(1) (2004) 47–70.
[26] R. Juanes and T.W. Patzek, Relative permeabilities for strictly hyperbolic models of three-phase flow in porous media, Transp. Porous Media 57(2) (2004) 125–152.

[27] M.J. King and A. Datta-Gupta, Streamline simulation: A current perspective, In Situ 22(1) (1998) 91–140.
[28] A. Kurganov, S. Noelle and G. Petrova, Semi-discrete central-upwind schemes for hyperbolic conservation laws and Hamilton–Jacobi equations, SIAM J. Sci. Comput. 23 (2001) 707–740.
[29] L.W. Lake, *Enhanced Oil Recovery* (Prentice-Hall, Englewood Cliffs, NJ, 1989).
[30] J.O. Langseth, N.H. Risebro and A. Tveito, A conservative front tracking scheme for 1D hyperbolic conservation laws, in: *Nonlinear Hyperbolic Problems: Theoretical, Applied, and Computational Aspects*, eds. A. Donato and F. Oliveri, Taormina (1992), Notes on Numerical Fluid Mechanics, Vol. 43 (Vieweg, Braunschweig, 1993) pp. 385–392.
[31] P.D. Lax, Hyperbolic systems of conservation laws II, Comm. Pure Appl. Math. 10 (1957) 537–566.
[32] T.-P. Liu, The Riemann problem for general 2×2 conservation laws, Trans. Amer. Math. Soc. 199 (1974) 89–112.
[33] D. Marchesin and B.J. Plohr, Wave structure in WAG recovery, Soc. Pet. Engrg. J. 6(2) (2001) 209–219.
[34] D.W. Pollock, Semianalytical computation of path lines for finite difference models, Ground Water 26 (1988) 743–750.
[35] G.A. Pope, The application of fractional flow theory to enhanced oil recovery, Soc. Pet. Engrg. J. 20(3) (1980) 191–205.
[36] N.H. Risebro, A front-tracking alternative to the random choice method, Proc. Amer. Math. Soc. 117(4) (1993) 1125–1129.
[37] N.H. Risebro and A. Tveito, Front tracking applied to a nonstrictly hyperbolic system of conservation laws, SIAM J. Sci. Statist. Comput. 12(6) (1991) 1401–1419.
[38] A. Sahni, R. Guzmán and M. Blunt, Theoretical analysis of three phase flow experiments in porous media, in: *SPE Annual Technical Conf. and Exhibition*, Denver, CO (SPE 36664) (6–9 October 1996).
[39] B.V. Shalimov, Filtration of a three-phase liquid (Buckley–Leverett model), Izv. Akad. Nauk SSSR Mekhan. Zhidk. i Gaza 7(1) (1972) 39–44 (in Russian, English translation in Fluid Dyn. 7 (1972) 36–40).
[40] L.F. Shampine and M.W. Reichelt, The MATLAB ODE suite, SIAM J. Sci. Comput. 18(1) (1997) 1–22.
[41] M. Shearer, Loss of strict hyperbolicity of the Buckley–Leverett equations for three phase flow in a porous medium, in: *Numerical Simulation in Oil Recovery*, ed. M.F. Wheeler (Springer, New York, 1988) pp. 263–283.
[42] M. Shearer and J.A. Trangenstein, Loss of real characteristics for models of three-phase flow in a porous medium, Transp. Porous Media 4 (1989) 499–525.
[43] Y.I. Stklyanin, The motion of a mixture of three liquids in a porous medium (in Russian), Izv. Akad. Nauk SSSR Otd. Tekhn. Nauk Mekhanika i Mashinostroenie 2(5) (1960).